Thin-Walled Structures 150 (2020) 105926

Contents lists available at ScienceDirect

Thin-Walled Structures

journal homepage: www.elsevier.com/locate/tws

Full length article

Efficient design of cold-formed steel bolted-moment connections for earthquake resistant frames

Jun Ye[a,b], Seyed Mohammad Mojtabaei[a,*], Iman Hajirasouliha[a], Kypros Pilakoutas[a]

[a] Department of Civil Engineering and Structural Engineering, The University of Sheffield, Sheffield, UK
[b] Department of Architectural and Civil Engineering, University of Bath, Bath, UK

ARTICLE INFO

Keywords:
Cold-formed steel sections
Bolted moment-resisting connection
Cyclic behaviour
FE analysis
Ductility

ABSTRACT

Cold-formed steel (CFS) sections can be designed in many configurations and, compared to hot-rolled steel elements, can lead to more efficient and economic design solutions. While CFS moment resisting frames can be used as an alternative to conventional CFS shear-wall systems to create more flexible space plans, their performance under strong earthquakes is questionable due to the inherited low local/distortional buckling of thin-walled CFS elements and limited ductility and energy dissipation capacity of typical CFS bolted-moment connections. To address the latter issue, this paper presents a comprehensive parametric study on the structural behaviour of CFS bolted beam-to-column connections with gusset plates under cyclic loading aiming to develop efficient design solutions for earthquake resistant frames. To simulate the hysteretic moment–rotation behaviour and failure modes of selected CFS connections, an experimentally validated finite element model using ABAQUS is developed, which accounts for both nonlinear material properties and geometrical imperfections. Connection behaviour is modelled using a connector element, simulating the mechanical characteristics of a bolt bearing against a steel plate. The model is used to investigate the effects of bolt arrangement, cross-sectional shape, gusset plate thickness and cross-sectional slenderness on the seismic performance of CFS connections under cyclic loading. The results indicate that, for the same amount of material, folded flange beam sections with diamond or circle bolt arrangements can provide up to 100% and 250% higher ductility and energy dissipation capacity, respectively, compared to conventional flat-flange sections with square bolt arrangement. Using gusset plates with the same or lower thickness as the CFS beam may result in a premature failure mode in the gusset plate, which can considerably reduce the moment capacity of the connection. The proposed numerical model and design configurations can underpin the further development and implementation of CFS bolted-moment connections in seismic regions.

1. Introduction

Compared to hot-rolled steel elements, cold-formed steel (CFS) thin-walled elements are easier to manufacture with a far greater range of section configurations. Having a high strength to weight ratio, they are easy to transport and erect and can lead to more efficient and economic design solutions. However, CFS sections are more prone to local/distortional buckling due to the large width-to-thickness ratio of their thin-walled elements. As a result, CFS cross-sections have traditionally been employed mainly as secondary load-carrying members such as roof purlins and wall girts. However, in the modern construction industry, CFS members are increasingly used as primary structural elements, especially in modular systems [1].

Conventional CFS structures usually comprise shear walls made of vertical studs, diagonal braces and top and bottom tracks. The performance of shear walls with different bracing systems such as straps, steel sheets, and K-bracing were evaluated experimentally on full-scale specimens under cyclic and monotonic loadings [2–4]. The results indicate that most of the shear wall systems tested can maintain their lateral and vertical load bearing capabilities up to the drift limits specified by most seismic codes. However, CFS shear walls may exhibit poor ductility due to the distortion buckling of the stud elements and the resulting rapid decrease in their load-bearing capacity [5]. Fiorino et al. [6] conducted shake table tests on a full-scale two-storey sheathing-braced CFS building, where the results demonstrated the acceptable seismic lateral resistance of these structures under seismic loads. However, monotonic and cyclic tests on full-scale strap-braced CFS walls showed that stud wall systems may exhibit a non-ductile seismic performance (e.g. due to

* Corresponding author.
E-mail address: smmojtabaei1@sheffield.ac.uk (S.M. Mojtabaei).

https://doi.org/10.1016/j.tws.2018.12.015
Received 24 July 2018; Received in revised form 26 October 2018; Accepted 11 December 2018
Available online 03 January 2019

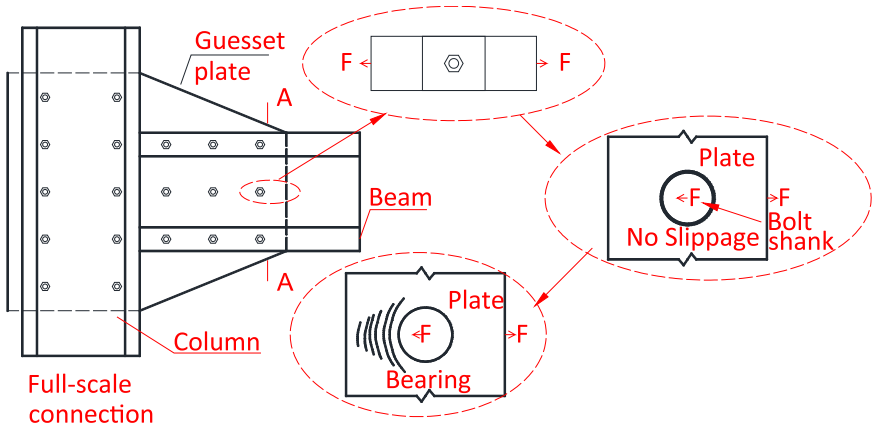

Fig. 1. Bearing behaviour of a single bolt against steel plate used in CFS bolted-moment connection.

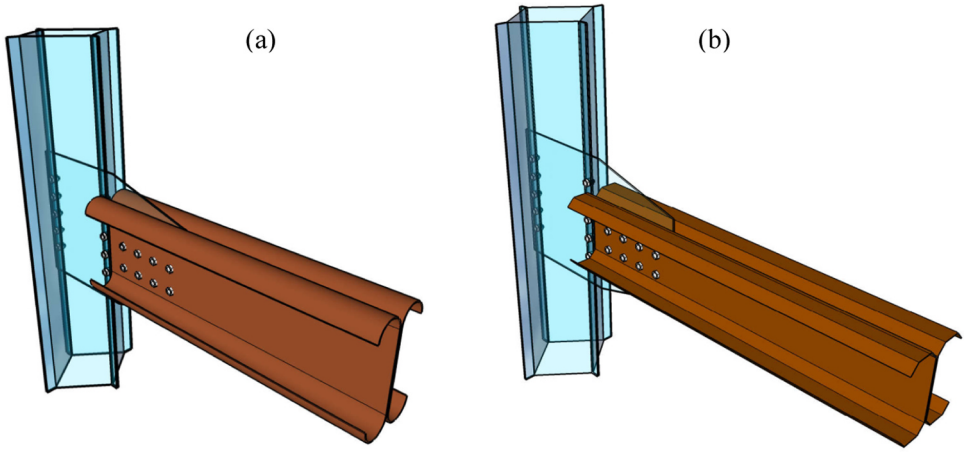

Fig. 2. Configuration of CFS moment resisting connections using gusset plate with (a) curved flange beam adopted from [22] and (b) folded flange beam adopted from [23].

gusset-to-track connection failure) [6].

CFS members have also been used as primary structural elements in low- to mid-rise multi-storey buildings [7] and CFS portal frames with bolted-moment connections [8,9]. Experimental and numerical investigations on bolted moment connections using CFS sections in general demonstrated their good strength and stiffness, and adequate deformation capacity for seismic applications [9,10]. However, the typical CFS bolted moment connections may exhibit very low ductility and energy dissipation capacity, especially when the width-to-thickness ratio of the CFS elements increases [11]. This highlights the need to develop more efficient CFS connections suitable for moment-resisting frames in seismic regions.

The global moment-rotation behaviour of CFS bolted connections is mainly governed by bolt distribution configuration, bolt tightening and bearing behaviour [12,13], as presented schematically in Fig. 1. Bolt slippage in CFS bolted connections can be avoided by appropriate tightening. The behaviour of beam-to-column CFS bolted moment resisting connections with gusset plates has been investigated experimentally and numerically under monotonic and cyclic loading conditions [12,14–18]. It was found that, though they usually exhibit a semi-rigid behaviour, they can generally provide enough stiffness and moment resistance for low to medium rise moment frames [18]. In another study, Lim et al. [9] examined experimentally the ultimate strength of bolted moment-connections between CFS channel-sections. The tested specimens included apex and eaves connections, and it was concluded that the connections exhibit a semi-rigid behaviour due to bolt-hole elongation in the thin-walled steel sheet. Analytical work by Lim et al. [10] indicated that bolt-group sizes in CFS connections can also have a significant impact on the bending capacity of connected sections. Based on the above studies, it can be concluded that the ductility and energy dissipation capacity of CFS bolted connections depend mainly on four factors: (a) material yielding and bearing around the bolt holes; (b) yielding lines resulting from the buckling of the CFS cross-sectional plates; (c) bolt distribution; and (d) cross-sectional shapes of the CFS beam elements. The effects of these factors will be investigated in this study.

Unlike the common misconception that slender CFS structural elements are not ductile, previous studies showed that by using an appropriate design CFS sections can offer significant ductility and energy dissipation capacity even when subjected to local/distortional buckling [19–21]. Experimental and analytical research on CFS moment resisting frames [22] at the University of Sheffield, UK, has also demonstrated that increasing the number of flange bends in CFS channel sections can delay the buckling behaviour. Follow-up studies proved that the optimised folded flange sections can provide up to 57% higher bending capacity [23] and dissipate up to 60% more energy through plastic deformations [24] compared to commercially available lipped channels. Consequently, higher strength, stiffness, and ductility can be potentially developed in CFS beams with an infinite number of bends (curved flange shown in Fig. 2(a)). Nevertheless, this type of cross-section is hard to manufacture and difficult to connect to typical floor systems. Considering the construction and manufacture constraints, the curved flange can be substituted with a folded flange cross-section (Fig. 2(b)). Both of these sections are examined in this study.

This paper aims to develop efficient design configurations for moment resisting CFS bolted beam-to-column connections to improve their

ductility and energy dissipation capacity and therefore facilitate their practical application in earthquake resistant frames. Detailed nonlinear FE models are developed by taking into account material nonlinearity, initial geometrical imperfections and bearing action which are known to affect the accuracy of the results [24]. The models also adopt a connector element to simulate the behaviour of a single bolt against the CFS plate. The developed FE models are verified against experimental results of CFS bolted connections under cyclic loading using test data by Sabbagh et al. [12]. An extensive parametric study is then conducted to investigate the effects of a wide range of design parameters including cross-sectional shapes, cross-sectional slenderness, bolt configuration and gusset plate thicknesses on the behaviour of the connections. Finally, the results are used to identify the most efficient design solutions to considerably improve the seismic performance of CFS bolted-moment connections.

2. Finite element model

Finite Element (FE) modelling is widely used to examine the behaviour of CFS bolted connections with gusset plates [9,25–30]. The results of previous studies in general demonstrate the adequacy of detailed FE models to predict the behaviour of CFS connections under monotonic [30,31] and cyclic loading [27]. This section describes the details of the FE models developed including the model proposed for simulating single bolt behaviour in a connection assembly. It should be noted that the bolt slippage can significantly change the cyclic behaviour of the CFS bolted connections [12]. Therefore, this study deals only with the CFS bolted moment connections without bolt slippage as a typical connection type in CFS frame systems. More information about FE modelling of the CFS connections with bolt slippage can be found in [27].

2.1. Bolt modelling

Lim and Nethercot [17,31] developed a simplified bolt model comprising of two perpendicular linear springs to model the bearing behaviour of a single bolt, and reported good agreement with experimental results of full-scale CFS joints subjected to monotonic loading. However, the linear spring elements used are not suitable for modelling the bearing behaviour of bolts under cyclic loads, due to nonlinearities in the bearing plate. Sabbagh et al. [27] used the connector element in ABAQUS [32] to model the behaviour of bolts under both monotonic and cyclic loading and achieved good agreement with experimental tests. Nonetheless, this approach induces stress concentrations around the two connector nodes. This issue can be overcome if the bolt behaviour is modelled explicitly using solid elements and surface-to-surface contact interactions [30,33,34]. The disadvantage of this is that it makes the model more complex and computationally expensive for cyclic modelling, especially when a large number of bolts is needed. Furthermore, convergence becomes an issue in the presence of bolt rigid body movement and slippage [34]. In this study, a simplified connection element which is similar to the concept of "component method" adopted by Eurocode 3 [35] is used to simulate the CFS full-scale connection behaviour. It is anticipated that the proposed model can provide accurate results with considerably lower computational costs compared to the complex FE models.

The point-based "Fastener" using a two-layer fastener configuration found in ABAQUS library [32] is employed to model individual bolts (see Fig. 3). Each layer is connected to the CFS beam and gusset plate using the connector element to define the interaction properties between the layers. To model the connector element, a "physical radius" r is defined to represent the bolt shank radius and simulate the interaction between the bolt and the nodes at the bolt hole perimeter. The adopted method can accurately capture the stress concentrations around the nodes at the bolt positions and help to simulate more accurately the bearing work of the bolts. As shown in Fig. 3, each fastener point is connected to the CFS steel plates using a connector element that couples the displacement and rotation of each fastener point to the average displacement and rotation of the nearby nodes. Hence, rigid behaviour is assigned to the local coordinate system corresponding to the shear deformation of the bolts. Fig. 4 shows the fasteners with connector elements modelled in a typical CFS bolted-moment connection. It should be mentioned that previous studies by D'Aniello et al. [36,37] highlighted the importance of accounting for the non-linear response of the bolts (e.g. due to shank necking or nut stripping) in the modelling of preloadable bolt assemblies. However, no bolt damage was observed in the reference experimental tests, and therefore, the failure modes of the bolts were not considered in this study.

2.2. Geometry, boundary conditions and element types

To model the CFS connections in this study, the general-purpose S8R element in ABAQUS [32] (8-noded quadrilateral shell element with reduced integration) is adopted. Shell elements in general can accurately capture local instabilities and have been successfully used by researchers to model CFS connections in bending [22,27]. Following a comprehensive mesh sensitivity study, the mesh size 20 × 20 mm is selected to balance accuracy and computational efficiency. The boundary conditions are defined to simulate the actual experimental test set-up used by Sabbagh et al. [12]. The translational degrees of freedom U_X and U_Y at the top of the back-to-back channel column are restrained, while the bottom of the column is considered to be pinned (see Fig. 5). Since in the experiments the back-to-back channel beams were assembled with bolts and filler plates, the web lines are tied together in the U_X, U_Y and U_Z directions using the "Tie" constraint in ABAQUS [32]. The out of plane deformation of beam (in X direction) is restrained at the location of the lateral bracing system of the test set-up (see Fig. 5). The column stiffeners (used in the experiments to ensure the column remains elastic) are tied to the column surfaces. While it was previously shown that deformation of panel zone can also contribute to the rotational response of bolted-moment connections [38,39], in this study it is assumed that the panel zone remains elastic during cyclic loading (due to the use of a thicker cross-section and column stiffeners). This is consistent with the experimental results reported by Sabbagh et al. [12]. To apply the external load, the nodes of the beam end section are coupled to their centroid using a coupling constraint.

2.3. Material model

The stress-strain behaviour of the CFS plate is simulated using the constitutive model suggested by Haidarali and Nethercot [40]. The stress-strain relationship consists of a Ramberg-Osgood equation up to the 0.2% proof stress, followed by a straight line with a slope of $E/100$ (where E is the elastic modulus taken as 210 GPa). This slope is obtained according to the coupon tests results reported by Sabbagh et al. [12], as shown in Fig. 6. The ultimate strain used here is 0.08. Mathematically, the stress-strain model is expressed as:

$$\varepsilon = \frac{\sigma}{E} + 0.002\left(\frac{\sigma}{\sigma_{0.2}}\right)^n \quad for \;\; \sigma \le \sigma_{0.2}$$
$$\varepsilon = \varepsilon_{0.2} + \frac{100(\sigma - \sigma_{0.2})}{E} \quad for \;\; \sigma \ge \sigma_{0.2} \tag{1}$$

where $\sigma_{0.2}$ is the 0.2% proof stress ($\sigma_{0.2} = 310MPa$), $\varepsilon_{0.2}$ is the strain corresponding to the 0.2% proof stress and n is a parameter determining the roundness of the stress-strain curve. The parameter n is taken as 10 to have the best agreement with the coupon test results. Fig. 6 compares the stress-strain curve from the coupon tests [12] with the material model used in this study.

Since the reference bolted-moment connection exhibited plastic deformations with strain reversals under the applied cyclic loading, the effect of cyclic strain hardening was taken into account in this study.

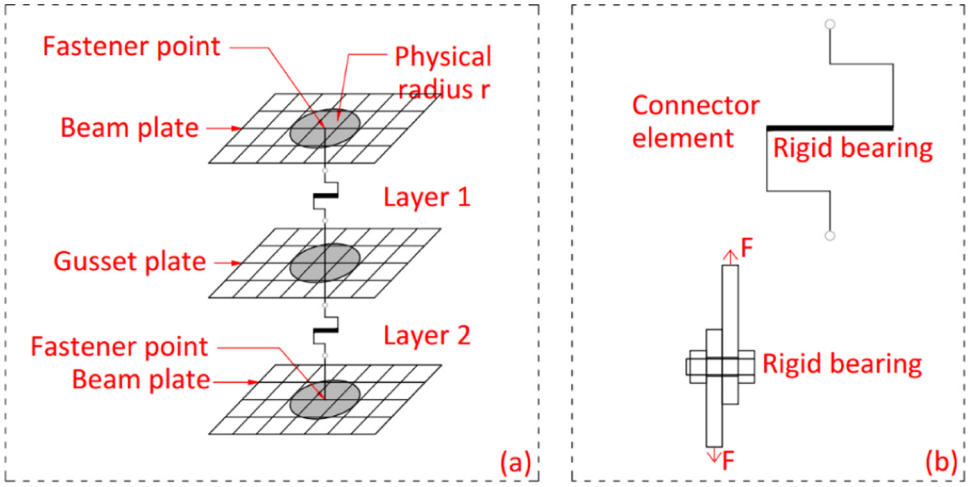

Fig. 3. Single bolt modelling in ABAQUS: (a) definition of fastener; (b) components defined in a connector section.

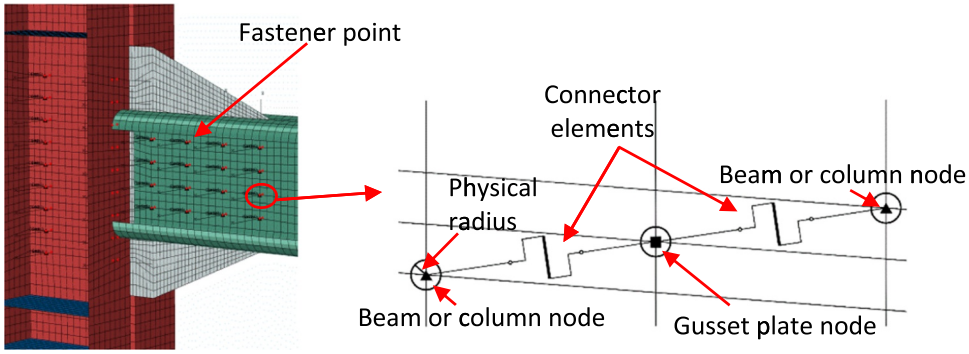

Fig. 4. FE model of the beam-column connection with fastener definition.

The combined hardening law in ABAQUS [32] was adopted based on the linear kinematic hardening modulus, C, determined as follows:

$$C = \frac{\sigma_u - \sigma_{0.2}}{\varepsilon_{pl}} \tag{2}$$

where $\sigma_{0.2}$ is the yield stress at the zero plastic strain and σ_u is a yield stress at ultimate plastic strain, ε_{pl}, all obtained from the monotonic coupon test results shown in Fig. 6. The adopted method is capable to take into account the Bauschinger effect [41,42] and has been shown to be efficient at simulating the cyclic behaviour of steel material with isotropic/kinematic hardening [27,43].

2.4. Imperfections

An experimental and analytical study carried out by Tartaglia et al. [39] showed that geometrical imperfections can significantly affect the cyclic response of an isolated beam leading to more severe strength degradation under both monotonic and cyclic loadings. Similarly,

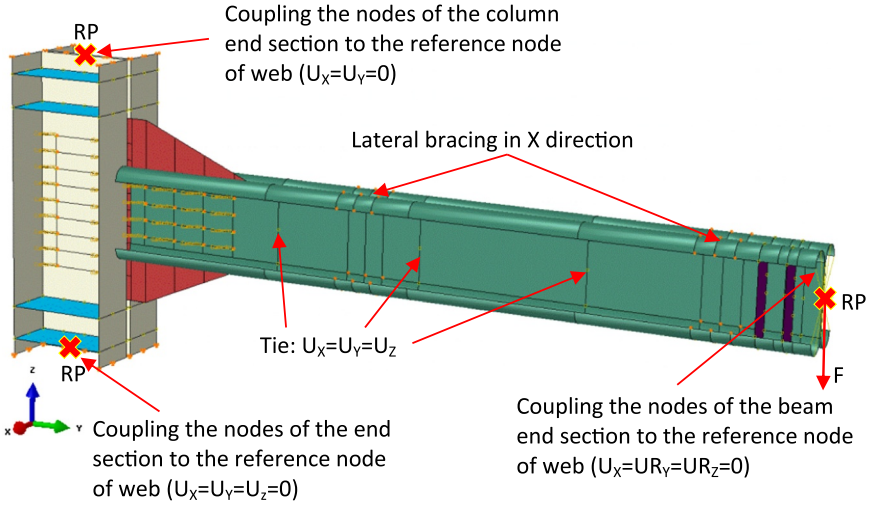

Fig. 5. Boundary conditions of the FE model for beam-column connections.

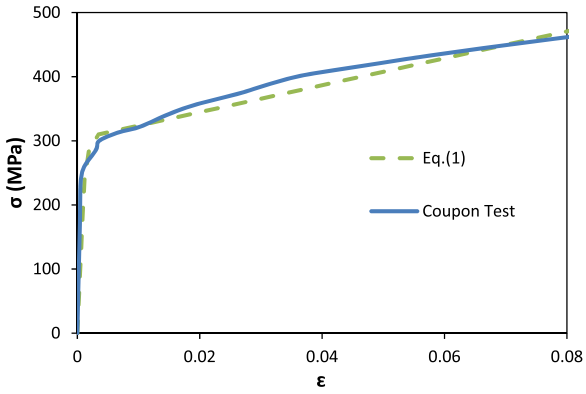

Fig. 6. Stress-strain curve used in the FE model.

previous studies have highlighted the importance of considering geometrical imperfections for more efficient design of both CFS sections (e.g. [44,45]). No global buckling (lateral-torsional buckling) was observed in the reference beam [12] due to the lateral bracing system used in the test setup. Therefore, in this study, depending on the critical buckling resistance, either local or distortional imperfection is incorporated into the FE models. For steel sheets with thickness (t) less than 3 mm, the imperfection amplitude is taken as $0.34t$ and $0.94t$ for the local and distortional imperfections, respectively, based on experimental and analytical work by Schafer and Peköz [46]. The selected amplitudes are adopted from 50% value of the Cumulative Distribution Function (CDF) of the experimentally measured imperfection data. For steel sheet thickness (t) larger than 3 mm, the imperfection magnitude is considered to be $0.3t\lambda_s$ based on the model proposed by Walker [47], where λ_s is the cross-sectional slenderness. It is worth mentioning that the Walker model can be considered as an upper bound for the data range presented by Schafer and Peköz [46]. The cross-sectional shape of the full CFS connection assembly, including CFS beam and column sections and gusset plate, with their corresponding imperfections are then generated by using an eigenvalue buckling analysis in ABAQUS [32]. The first buckling mode of the CFS connection is used to find the general shape of the local and distortional imperfections. This general shape is then scaled by the imperfection amplitude and superimposed to obtain the initial state of the CFS connection, as shown in Fig. 7.

2.5. Solution technique and loading regime

Nonlinear FE analyses are conducted using Static General Analysis (available in ABAQUS library) by applying a displacement at the reference point placed on the beam end section as show in Fig. 5. The AISC 341-16 [48] cyclic loading regime used in the reference experimental tests [9] is adopted as shown in Fig. 8.

2.6. Validation of adopted FE modelling approach

Fig. 9 shows the moment-rotation hysteresis behaviour of the CFS connection test A1 [49], which is used to validate the developed FE models. This connection was designed to prevent bolt slippage by providing sufficient friction force between the steel plates through pretensioning the bolts with a torque of 240 N m [49]. The simplified bolt model in Fig. 3 is used for modelling of the bolts (the radius of the bolts was 18 mm). The experimental and FE responses subjected to cyclic loading are presented in terms of moment-rotation (M-Θ) hysteretic curves in Fig. 9. The numerical results show a very good agreement with the corresponding experimental measurements. For better comparison, Fig. 10 compares the failure shape of the modelled connection under cyclic loads with the experimental observations. The von Mises stress distribution extracted from FE analysis is shown in Fig. 10(a) with grey areas indicating yielding. It should be noted that the stress and in-plane deformations developed in gusset plate is noticeably smaller than CFS beam due to its thicker plate thickness. It is shown that the developed numerical model captures successfully the shape and the position of local/distortional buckling in the CFS beam. These results validate the modelling approach used in this study.

3. Design parameters

The main design parameters examined are beam cross-sectional shape, plate thickness (or cross-sectional slenderness), bolt configuration and gusset plate thickness. Considering the capabilities of the cold-rolling and press-braking processes to provide cross sections with intermediate stiffeners or folded plates, four different geometries including flat, stiffened flat, folded and curved shaped channel cross-sections are selected for the parametric study, as shown in Fig. 11. For each cross-section, four different plate thicknesses of 1, 2, 4, 6 mm are used. The selected cross-sections have the same total plate width, and

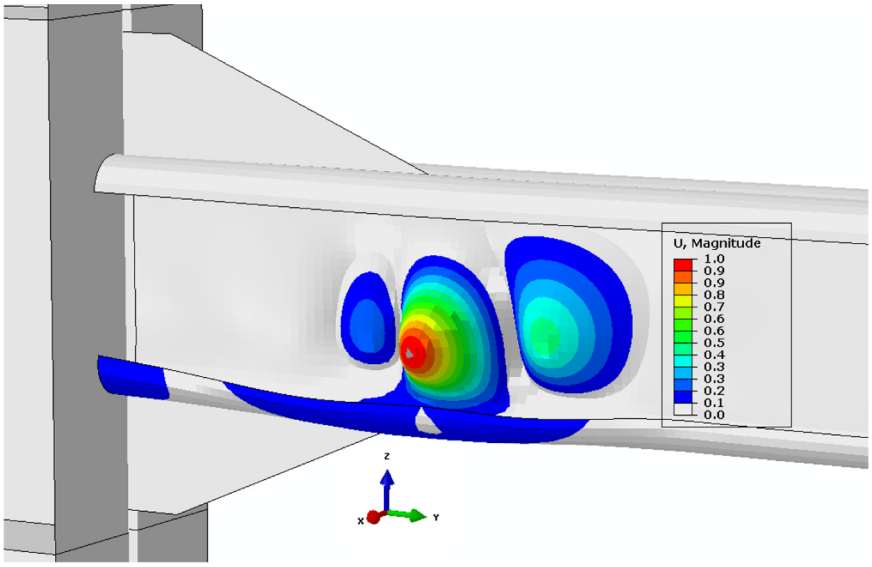

Fig. 7. First buckling mode shape of elastic buckling analysis used to obtain the geometric imperfections.

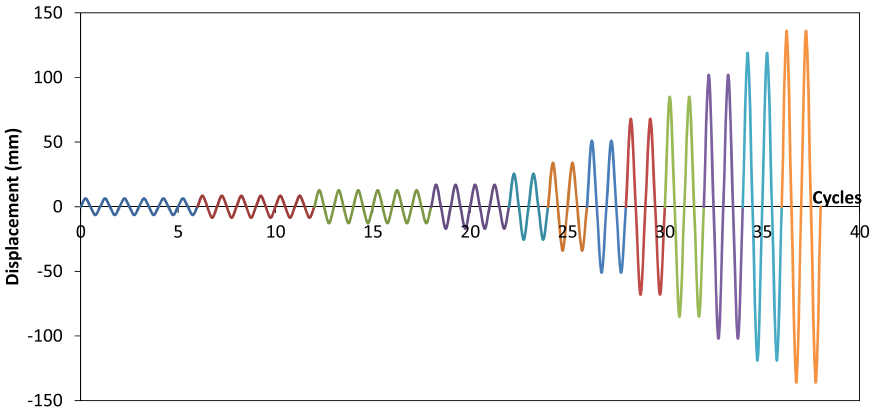

Fig. 8. Cyclic loading regime for the reference experimental test [12] and numerical study.

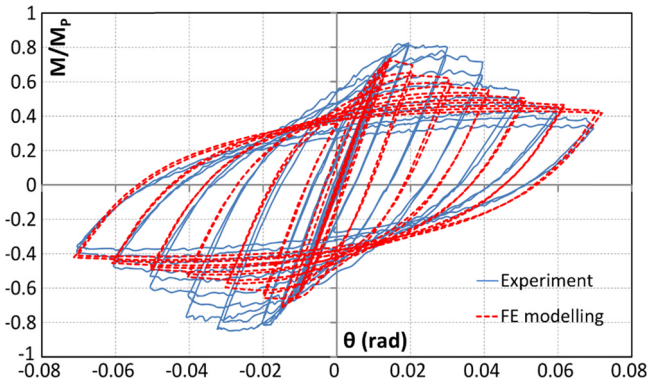

Fig. 9. Comparison between tested moment-rotation hysteretic curve of connection A1 [49] and the results of FE modelling.

therefore, use the same amount of structural material. Moreover, to investigate the effect of different flange shapes, all cross-sections are designed to have a similar web slenderness ratio. It should be mentioned that the curved flange cross-section in this study is less practical and is mainly used for comparison purposes and verification of analytical models with experimental results [12]. Also thin walled sections with curved or folded flange cross sections may be sensitive to crippling due to support transvers actions from joints and purlins, which should be considered in the design process of these elements.

Since bolt distribution can also affect the stress field distribution of bolted moment connections [10], three types of bolt distributions including circle, diamond and square shapes are selected, as shown in Fig. 12. To increase the efficiency of the proposed connection, the number of bolts and their arrangement were also optimised in this study. As a result, the number of required bolts was reduced from 16 in the reference experimental tests [12] to 9 bolts. It is worth mentioning that circular bolt arrangement may be less practical compared to square and diamond in real constructional practice, however, in this study it is investigated for comparison purposes. The effect of gusset plate thicknesses on the cyclic behaviour of the bolted CFS connections is also investigated in the parametric study. It should be noted that, for better comparison, the performance parameters of the sections with different shapes and plate thicknesses are presented as a function of their slenderness ratio calculated as:

$$\lambda_s = \sqrt{\frac{f_y}{\sigma_{cr}}} \tag{3}$$

where σ_{cr} and f_y are the critical buckling stress and yield stress, respectively.

4. Cross-sectional classification of CFS beams

4.1. Eurocode regulations

To design CFS beams for bending, Eurocode 3 [50,51] divides the cross-section of CFS beam elements into individual plates subjected to either compression, bending or combined bending and compression. Each plate is identified as internal or outstand element according to the edge boundary conditions. Based on their susceptibility to local buckling, sections are categorized into four different classes (1, 2, 3 and 4). This classification is based on the slenderness of the constituent flat elements (width to thickness ratio), yield stress, edge boundary conditions and applied stress gradient. The overall classification of a cross-section is obtained using the highest (most unfavourable) class of its compression parts. Table 1 lists the Eurocode 3 classifications obtained for channels with flat, stiffened flat and folded flanges used in this study. It should be noted that the Eurocode classification cannot be applied directly to sections with round elements (e.g. curved-flange channel).

As shown in Fig. 13, the concept of the Eurocode cross-sectional classification is based on the moment-rotation ($M-\theta$) curves of the elements, where M_y, M_p and M_u represent yield moment, plastic moment and peak moment capacity, respectively. Class 1 cross-sections can form a plastic hinge with the rotation capacity obtained from plastic analysis without reduction of their resistance ($M_p < M_u$). Class 2 cross-sections are capable of developing their full plastic moment resistance, but have limited rotation capacity due to local buckling ($M_p < M_u$). In class 3 cross-sections, the stress in the extreme compression fibre reaches the yield strength, but local buckling prevents the development of the plastic moment resistance ($M_y < M_u < M_p$). In class 4 cross-sections, local buckling occurs before the attainment of yield stress in one or more parts of the cross-section ($M_u < M_y$). Since the moment-rotation response of class 1 and class 2 sections follow a similar trend ($M_p < M_u$), the two classes can be distinguished based on the pure plastic rotation capacity factor (R) in EN 1993-1-1 [50]:

$$R = \frac{\theta_u - \theta_p}{\theta_p} \tag{4}$$

where θ_u is the ultimate rotation corresponding to the drop in the moment-rotation curve in the softening branch, and θ_p is the rotation corresponding to the plastic moment at the hardening branch, as shown in Fig. 13.

4.2. Classification based on moment-rotation behaviour

The Eurocode 3 cross-sectional classification concept is assessed here by examining the predicted moment-rotation behaviour under

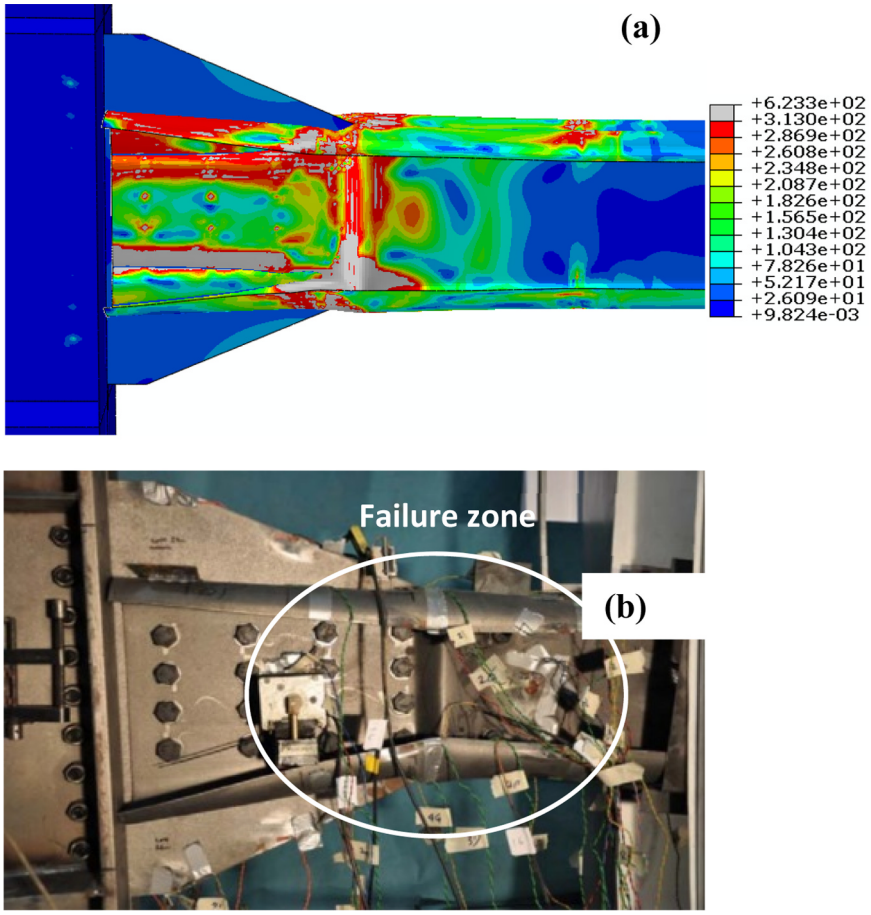

Fig. 10. Comparison between tested and analysed buckled shape of the connection A1: (a) FE von Mises stress distribution, and (b) Experimental observation (adopted from [49]).

monotonic load. Non-linear inelastic post-buckling analyses (Static Riks) are performed on 2 *m* long CFS cantilevers, using single channel cross-sections, as shown in Fig. 14. The CFS members are fully fixed at one end and are subjected to a tip load at the centroid of the other end. The centroid is coupled to the beam end cross-section and boundary conditions are applied to prevent the lateral movement of the flanges at 1/3 length intervals (see Fig. 14). Other FE modelling parameters (e.g. mesh size, material properties and geometric imperfections) are as described in Section 2.

Fig. 15 illustrates how the cross-section classification is applied based on normalised moment and pure plastic rotation capacity factor (R). As shown in Table 1, all of the sections with 1, 2, 4, and 6 mm plate thickness are identified as class 4, 3, 2 and 1, respectively. The Eurocode slenderness limits for class 1 and 4 channel sections are found to be in general sufficient, but they are not very accurate for class 2 and 3 channel sections.

Cross-sectional classifications may also be determined using the classical finite strip method [52,53], which estimates the buckling capacity of thin-walled members by taking into account local, distortional and global buckling elastic modes. The critical elastic buckling stress of the cross-sectional shapes used in this study (subjected to bending) are determined based on the minimum of the local buckling (σ_l) and the distortional buckling (σ_d) stresses obtained from constrained finite strip software CUFSM [54]. Due to the presence of the lateral supports, the

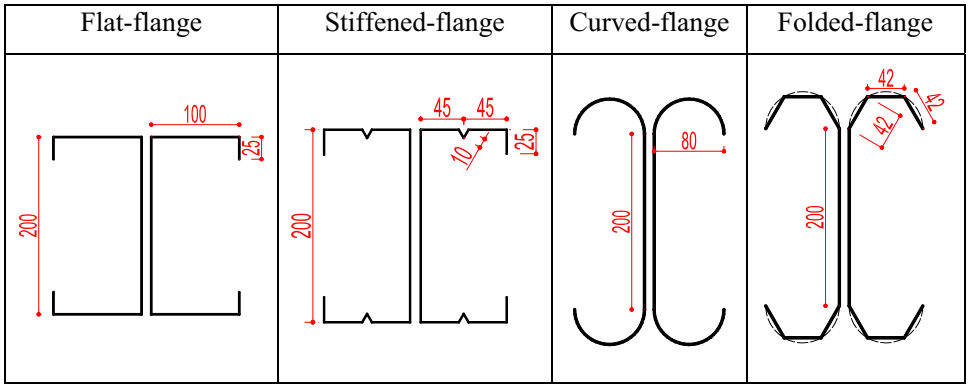

Fig. 11. Details of the back-to-back beam cross-sectional dimensions (in mm), L = 2000 mm.

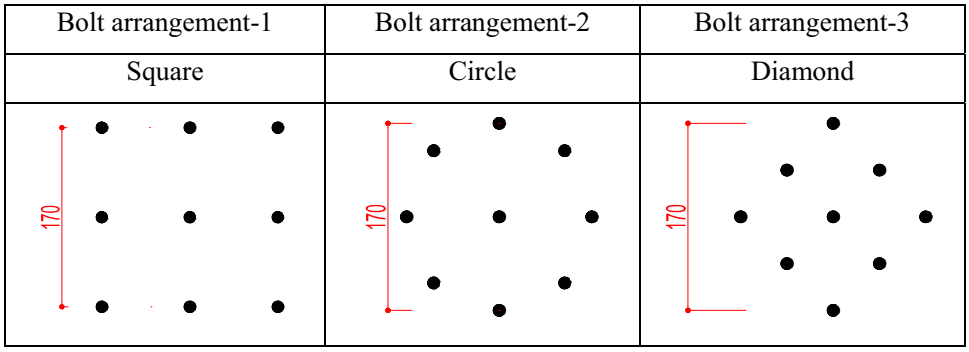

Fig. 12. Different bolt arrangements.

global buckling mode is not considered to be dominant in this study (see Fig. 14). The critical buckling stresses obtained for the different cross sections are presented in Table 1. It is shown that the ratio of the critical stress to the yield stress is in the range of 3–6, 2–3 and 1–1.5 for class 1, 2 and 3 sections, respectively. For class 4 sections, local buckling is always identified as the dominant buckling mode and the critical buckling stress is generally smaller than the yield stress. This indicates that the critical buckling stress can be also used as a simple measure to identify the cross-sectional classification based on Eurocode 3.

5. Efficiency of CFS bolted-moment connections

In this section, the results of the parametric study are used to identify efficient design solutions for CFS bolted-moment connections.

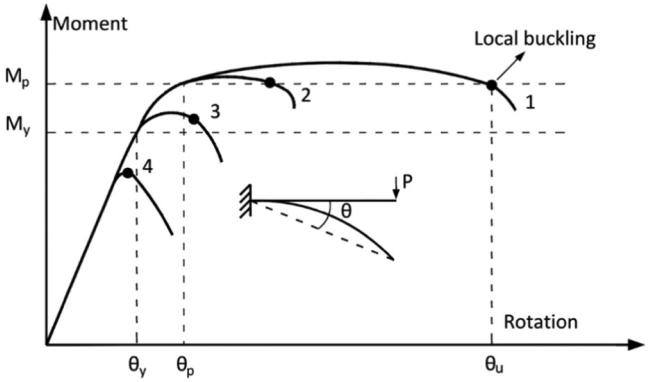

Fig. 13. Cross-sectional classification based on moment-rotation curves.

Table 1
Cross-sectional classification of the CFS cross-sections.

Section	Plate Thickness (mm)	Eurocode classification based on slenderness limits					Eurocode concept	Finite Strip Method
		Flanges		Lips	Web	Overall		
		Internal	Outstand					
Flat	1	4	-	4	4	4	4	$\sigma_l = 0.2794 f_y$ Local
	2	4	-	3	3	4	3	$\sigma_d = 1.0633 f_y$ Distortional
	4	1	-	1	1	1	2	$\sigma_d = 2.3122 f_y$ Distortional
	6	1	-	1	1	1	1	$\sigma_d = 3.7827 f_y$ Distortional
Stiffened Flat	1	4	-	4	4	4	4	$\sigma_l = 0.5029 f_y$ Local
	2	1	-	3	3	3	3	$\sigma_d = 1.1994 f_y$ Distortional
	4	1	-	1	1	1	2	$\sigma_d = 2.6401 f_y$ Distortional
	6	1	-	1	1	1	1	$\sigma_d = 4.3095 f_y$ Distortional
Folded	1	4	4	-	4	4	4	$\sigma_l = 0.3995 f_y$ Local
	2	1	4	-	3	4	3	$\sigma_d = 1.4895 f_y$ Distortional
	4	1	3	-	1	3	2	$\sigma_d = 3.2351 f_y$ Distortional
	6	1	1	-	1	1	1	$\sigma_d = 5.2191 f_y$ Distortional
Curved	1	-	-	-	4	-	4	$\sigma_l = 0.5808 f_y$ Local
	2	-	-	-	3	-	3	$\sigma_d = 1.6887 f_y$ Distortional
	4	-	-	-	1	-	2	$\sigma_d = 3.6603 f_y$ Distortional
	6	-	-	-	1	-	1	$\sigma_d = 5.896 f_y$ Distortional

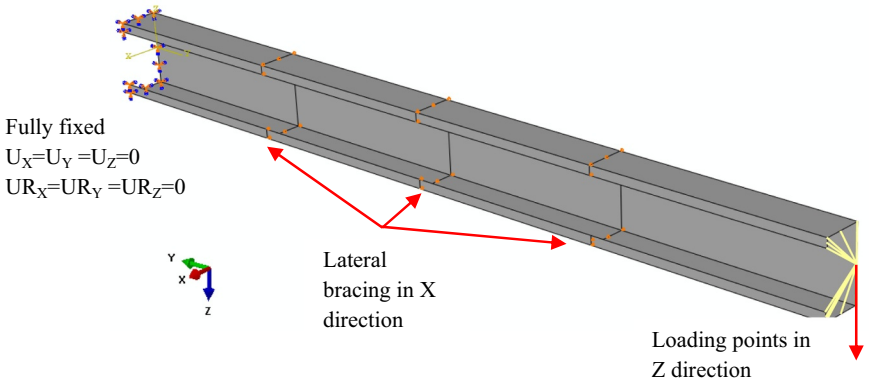

Fig. 14. Typical boundary conditions, constrains and loading point of cantilever channels.

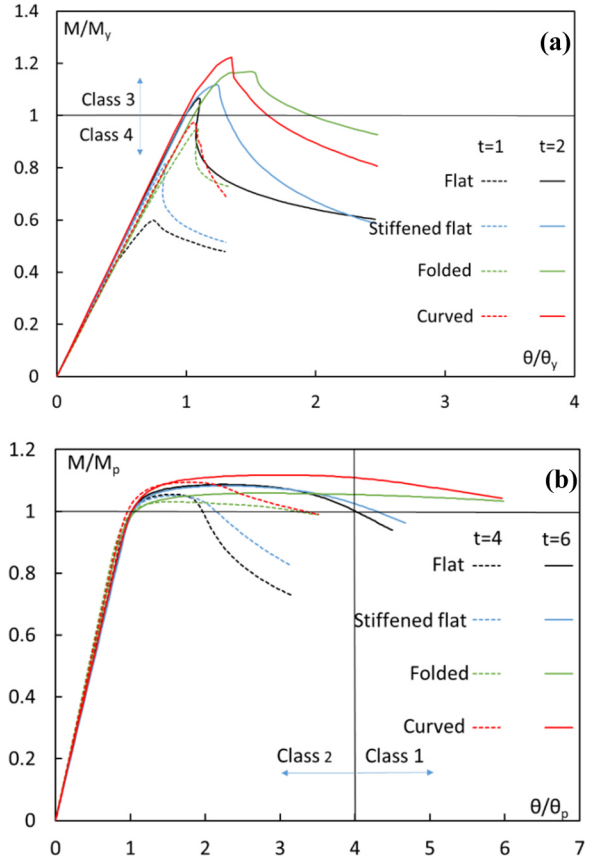

Fig. 15. Normalised moment–rotation responses for cross-section classification: (a) t = 1 mm and 2 mm and (b) t = 4 mm and 6 mm.

5.1. Moment-rotation behaviour

Fig. 16 compares the cyclic response and the cyclic moment-rotation envelope of the flat flange channels with circle bolt arrangement and various plate thicknesses (1, 2, 4 and 6 mm). The cyclic moment-rotation envelope is specified in both positive and negative rotations by plotting the locus of peak moment points at the first cycle of each load amplitude. It should be noted that, unlike a monotonic moment rotation backbone curve, the cyclic moment-rotation envelope can take into account the strength degradation due to cyclic loading as observations in the experimental results conducted by Padilla-Llano et al. [20,21]. The rotation of the connection was quantified as the ratio of beam tip displacement to the length of the beam up to the gusset plate. The moment-rotation results are used to determine different performance parameters such as moment capacity, yield moment, ductility, energy dissipation capacity and equivalent viscous damping coefficient in the following sections.

The initial stiffness of a CFS bolted-moment connection, $S_{j,ini}$, can be used to classify the rigidity of the connection based on Eurocode 3 part 1–8. The connections with $S_{j,ini} \times (\frac{L_b}{EI_b})$ less than 0.5, between 0.5 and 25 and over 25 are classified as “simple”, “semi-rigid” and “rigid”, respectively, where L_b is the beam length and EI_b is the flexural rigidity of the beam. Table 2 lists the rigidity of the different connections used in this study. The results indicate that connections with cross-sectional classes 1 and 2 are always classified as “rigid”, while those with cross-sectional classes 3 and 4 should be treated as “semi-rigid”.

5.2. Failure mode

The failure modes of the bolted-moment CFS connections obtained from the detailed FE models are identified in Table 2. It is shown that, in general, the dominant mode is local buckling of the CFS beam section close to the first row of the bolts. This can be attributed to the effect of bolt group on the stress distribution at the connection zone. The results indicate that for flat and stiffened flat channels, local buckling occurs at both web and flange of the CFS section. But using curved and folded flange channels can postpone the local buckling of the flange by creating an in-plane stiffness through arching action and shifting the local buckling failure to the web. Fig. 17 shows the typical failure mode of the beams with flat and bent flange channel sections.

5.3. FEMA bi-linear idealisation model

To characterize the cyclic behaviour of the selected bolted-moment connections, FEMA model [55] is developed based on the cyclic moment-rotation envelope, which is capable to take into account both positive and negative post-yield slopes. As shown in Fig. 18, FEMA model uses an ideal bi-linear elastic plastic response to represent the non-linear behaviour of an assembly by incorporating an energy balance approach. The area below the cyclic moment-rotation envelope curve is assumed to be equivalent to the area under the idealised bi-linear FEMA curve.

The yield rotation (θ_{y1}) is determined on the condition that the secant slope intersects the actual envelope curve at 60% of the nominal yield moment (M_{y1}), while the area enclosed by the bilinear curve is equal to that enclosed by the original curve bounded by the target displacement (θ_t). The target rotation was assumed to be corresponding to the rotation at which the flexural capacity of the system dropped by 20% (i.e. $\theta_t = \theta_u$), also recommended by AISC [48]. The characteristic parameter values of the FEMA models corresponding to the different bolted-moment CFS connections are presented in Table 2. For better comparison between the behaviour of different types of connections, Table 2 also presents the yield moment results calculated based on the FEMA idealised bi-linear curve up to the rotation at the maximum

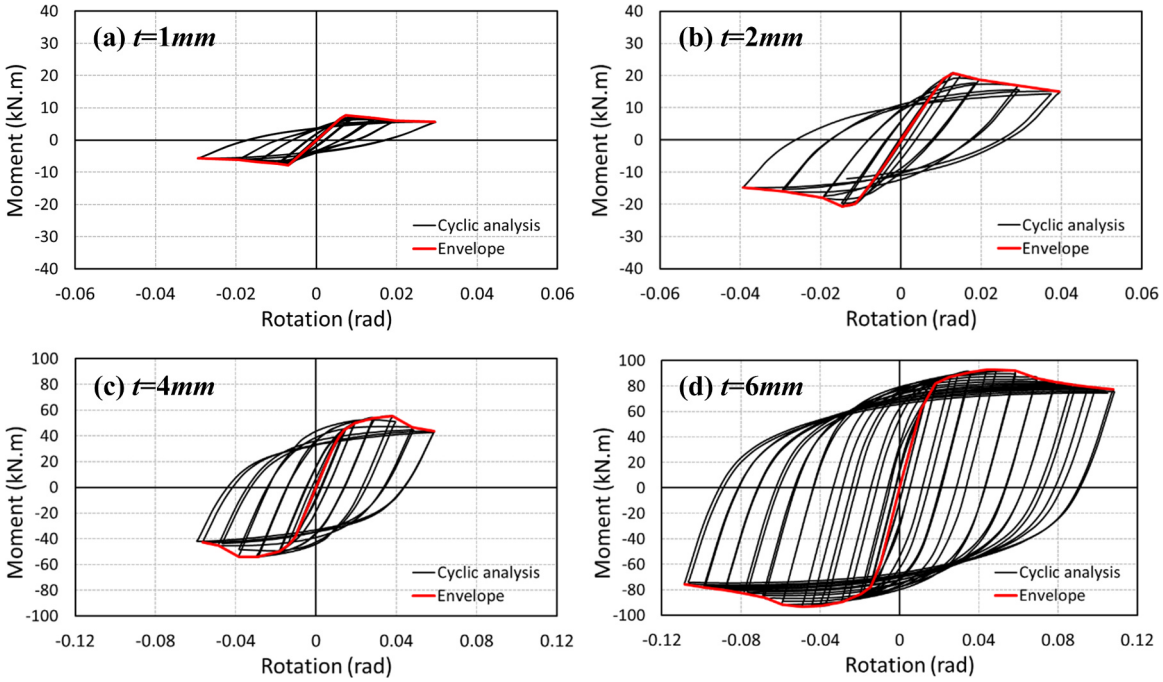

Fig. 16. Cyclic moment-rotation relationship and envelope curves of the connections with flat flange beam section and circular bolt arrangement.

moment capacity (M_{y2}).

5.4. Moment capacity of the connections

Fig. 19 compares the moment capacity of the CFS connections with different cross-sections, plate thicknesses and bolt arrangements. While previous studies showed that CFS channels with folded-flange and curved-flange sections can generally provide considerably higher flexural moment capacity compared to standard lipped channels [12,23], the results in Fig. 19 indicate that using bent flange channels (folded and curved) can only increase the moment capacity of the connections by up to 10%. There are two main reasons for this contradiction: (i) The bolts placed in the web result in the reduction of the moment-capacity of the channel-sections at the connection zone due to the bi-moment effects [10]. Bi-moment is equal to the product of the major axis moment and the eccentricity of the web centreline from the shear centre and puts each flange into bending about its own (horizontal) plane. (ii) Using channels with deep web reduces the effects of the flange on the moment capacity of the connections, since bending moments cannot be transferred directly from web to flanges. As shown in Fig. 19, the slenderness of the CFS beam elements and the arrangement of the bolts seem to be the most important design parameters affecting the capacity of the connections. In general, using a square bolt arrangement leads to a higher bending moment capacity especially in the case of CFS beam elements with low slenderness ratios (class 1 and 2), where up to 32% increase is observed compared to the other bolt arrangements.

5.5. Seismic resistance requirements

American Institute of Steel Construction (AISC) [48] imposes some performance requirements for beam-to-column connections in seismic force resisting systems. For special moment frames (SMFs), AISC stipulates that the bolted-moment connections should be able to undergo at least 0.04 rad rotation with less than 20% drop from their peak moment (M_u). It is shown in Table 2 that the bolted-moment connections with beam sections class 1 and 2 (plate thicknesses of 4 and 6 mm) can satisfy the AISC requirements for SMFs. Connections with beam class 2 (plate thicknesses of 2 mm) are only acceptable when intermediate stiffeners are used in the flanges (stiffened flat). The results show that the connections with class 4 beam cross sections (plate thicknesses of 1 mm) are not suitable for SMFs in seismic regions.

5.6. Ductility ratio of the connections

Moment resisting connections in seismic resisting systems should provide enough ductility to withstand and redistribute the seismic loads. The fundamental definition of ductility ratio (μ) is the ratio of the ultimate rotation (θ_u) to the yield rotation (θ_y), as follows:

$$\mu = \theta_u/\theta_y > 1 \quad (5)$$

The ductility ratio of the CFS connections in this study is calculated based on the results of the FEMA bi-linear idealisation models by using the rotation at 80% of the post-ultimate moment as the ultimate rotation (see Fig. 18). The ductility ratios of the connections with different beam cross-sections, plate thickness and bolt arrangements are compared in Fig. 20. It can be observed that the connection ductility ratio is highly affected by the beam cross-sectional shape and slenderness ratio as well as bolt distribution. In general, the ductility of the connections increases by decreasing the slenderness ratio of the CFS beam. This increase is particularly high for beams with lower slenderness ratios (higher classes). The results show that in most cases the connections with class 1 and 2 beam sections provide a good level of ductility suitable for seismic applications. This conclusion is in agreement with the AISC requirement checks presented in Section 5.5.

As shown in Fig. 20, for the same beam slenderness ratio and bolt arrangement, folded flange sections generally result in the highest ductility ratios, up to 55%, 45% and 30% higher than curved, flat and stiffened flat sections, respectively. The best bolt arrangement appears to be governed by beam slenderness ratio (or classifications) and cross-sectional shape. For folded and curved flange class 1 and 2 channels, diamond bolt arrangement provides the highest ductility ratios, while for class 3 and 4 channels the circle bolt arrangement leads to the best results. For CFS beams with flat and stiffened flat flanges, the circle bolt arrangement results in the highest ductility ratio for all cross-section classifications. It is worth mentioning that, in general, using the circle and diamond bolt arrangements can significantly increase the ductility of the connections (by up to 100%) compared to the conventional square bolt arrangement, especially for the sections with lower

Table 2
Characteristic parameters of the CFS connections using FEMA models.

Bolt Configuration	Plate Thickness (*mm*)	Beam type	Yield moment M_{y2} (*kN m*)	Yield moment M_{y1} (*kN m*)	Yield rotation θ_{y1} (*rad*)	Ultimate rotation (*rad*)	Buckling mode [a]	AISC SMF	Connection Rigidity (EN 1993-1-8)
Circle	1	Flat	6.9	5.8	0.006	0.013	LW-LF	×	Semi-Rigid
		Stiffened flat	6.9	6	0.006	0.018	LW-LF	×	
		Folded	7.6	6.4	0.006	0.014	LW	×	
		Curved	7.9	7	0.006	0.010	LW	×	
	2	Flat	20.8	20.1	0.011	0.029	LW-LF	×	Semi-Rigid
		Stiffened flat	20.9	21.8	0.012	0.049	LW-LF	✓	
		Folded	21.6	23.1	0.011	0.039	LW	×	
		Curved	24.0	23.3	0.010	0.030	LW	×	
	4	Flat	48.3	55.3	0.015	0.059	LW-LF	✓	Rigid
		Stiffened flat	48.7	54.6	0.015	0.066	LW-LF	✓	
		Folded	51.7	60.0	0.014	0.057	LW	✓	
		Curved	59.6	65.8	0.014	0.049	LW	✓	
	6	Flat	82.9	93.4	0.015	0.118	LW-LF	✓	Rigid
		Stiffened flat	83.4	94.6	0.016	0.125	LW-LF	✓	
		Folded	95.3	103.6	0.015	0.116	LW	✓	
		Curved	98.5	111.1	0.014	0.079	LW	✓	
Diamond	1	Flat	7.1	5.7	0.007	0.010	LW-LF	×	Semi-Rigid
		Stiffened flat	7.1	5.9	0.007	0.015	LW-LF	×	
		Folded	7.8	6.2	0.007	0.015	LW	×	
		Curved	8.0	7.4	0.007	0.009	LW	×	
	2	Flat	18.7	19.9	0.012	0.029	LW-LF	×	Semi-Rigid
		Stiffened flat	19.6	20.6	0.012	0.038	LW-LF	×	
		Folded	20.8	22.1	0.011	0.039	LW	×	
		Curved	24.5	24.6	0.011	0.019	LW	×	
	4	Flat	46.4	53.1	0.016	0.059	LW-LF	✓	Rigid
		Stiffened flat	46.9	51.1	0.015	0.068	LW-LF	✓	
		Folded	49.0	56.3	0.014	0.066	LW	✓	
		Curved	52.1	62.1	0.015	0.059	LW	✓	
	6	Flat	76.4	87.3	0.015	0.108	LW-LF	✓	Rigid
		Stiffened flat	76.8	87.6	0.015	0.117	LW-LF	✓	
		Folded	84.3	94.5	0.015	0.147	LW	✓	
		Curved	92.9	105.2	0.015	0.097	LW	✓	
Square	1	Flat	7.6	6.8	0.006	0.007	LW-LF	×	Semi-Rigid
		Stiffened flat	7.7	6.6	0.006	0.020	LW-LF	×	
		Folded	7.9	7.3	0.005	0.018	LW	×	
		Curved	8.2	7.8	0.005	0.011	LW	×	
	2	Flat	23.6	23.4	0.011	0.020	LW-LF	×	Semi-Rigid
		Stiffened flat	23.8	23.7	0.011	0.040	LW-LF	✓	
		Folded	24.2	26.0	0.010	0.038	LW	×	
		Curved	26.3	26.3	0.010	0.019	LW	×	
	4	Flat	54.5	62.5	0.015	0.041	LW-LF	✓	Rigid
		Stiffened flat	55.0	60.8	0.015	0.058	LW-LF	✓	
		Folded	59.6	69.5	0.014	0.059	LW	✓	
		Curved	62.1	69.8	0.013	0.040	LW	✓	
	6	Flat	101.0	118.4	0.017	0.058	LW-LF	✓	Rigid
		Stiffened flat	104.4	118.7	0.018	0.069	LW-LF	✓	
		Folded	112.9	133.6	0.015	0.088	LW	✓	
		Curved	115.2	123.7	0.014	0.069	LW	✓	

[a] LF: Local buckling in flange; LW: Local buckling in web.

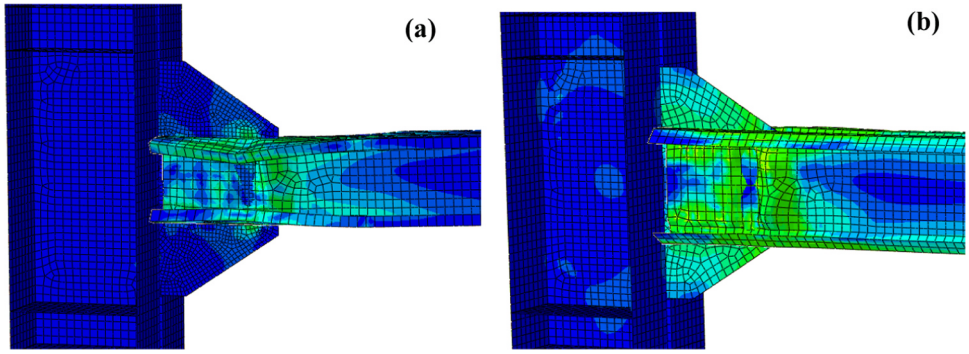

Fig. 17. Typical failure modes: (a) flat flange channel, (b) bent flange channel.

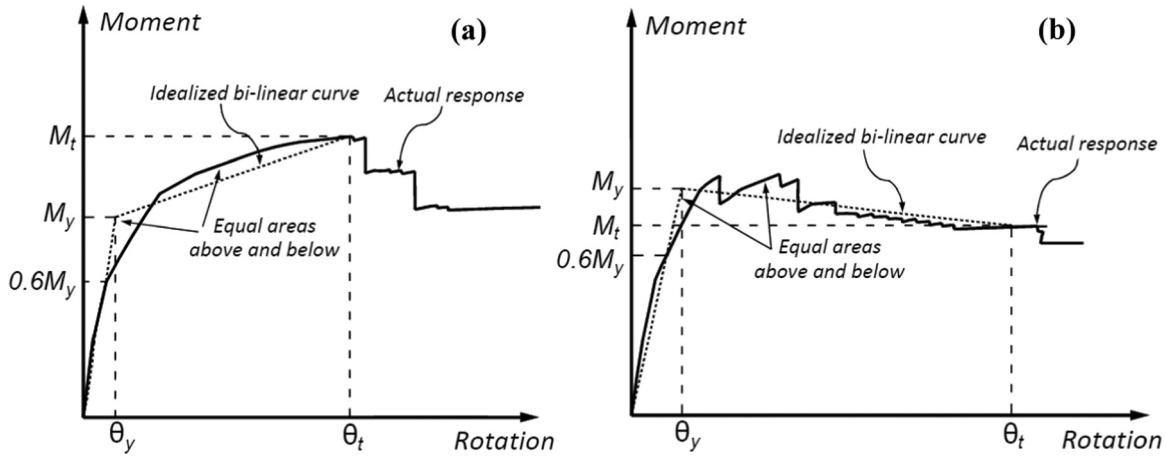

Fig. 18. FEMA bi-linear idealisation model: (a) Positive post-yield slope, (b) Negative post-yield slope.

slenderness ratios.

5.7. Energy dissipation

The seismic performance of structures can be improved considerably by increasing the energy dissipation in the structural elements and connections. For each connection, the area under the FEMA bi-linear idealisation curve of the moment-rotation hysteretic response (see Section 5.3) is used to calculate the energy dissipation capacity of the connection, as shown in Fig. 21. The results indicate that the effect of cross-sectional shape and bolt configuration on the energy dissipation capacity of the connections is only evident when class 1 beam cross-sections with lower slenderness ratios are utilized. It should be noted that class 3 and 4 beam sections do not reach their plastic moment capacity (due to premature cross-sectional buckling), and therefore, their ability to dissipate energy is very limited. On the contrary, CFS class 1 sections can exhibit up to 3 times higher plastic rotations compared to the other sections (see Section 4.2), and hence show a much higher energy dissipation capacity.

Folded flange beam cross sections in the connections result in up to 250%, 200% and 150% higher energy dissipation capacity compared to the flat, curved and stiffened flat sections, respectively. In general, diamond and circle bolt configurations can considerably increase (up to 164%) the energy dissipation capacity of the connections with class 1 beam cross sections compared to the conventional square bolt arrangement. These conclusions are in good agreement with the ductility results presented in the previous section.

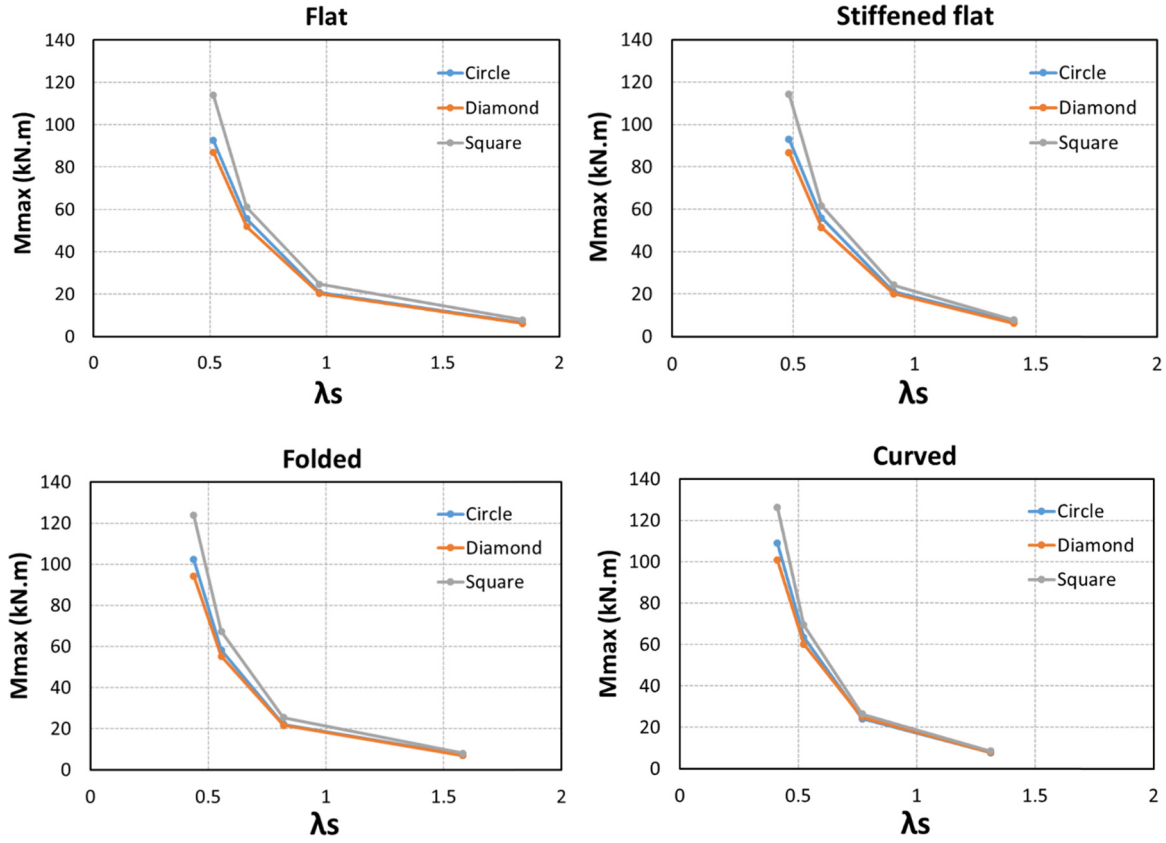

Fig. 19. Moment capacity of CFS connections as a function of slenderness ratio and bolt arrangement.

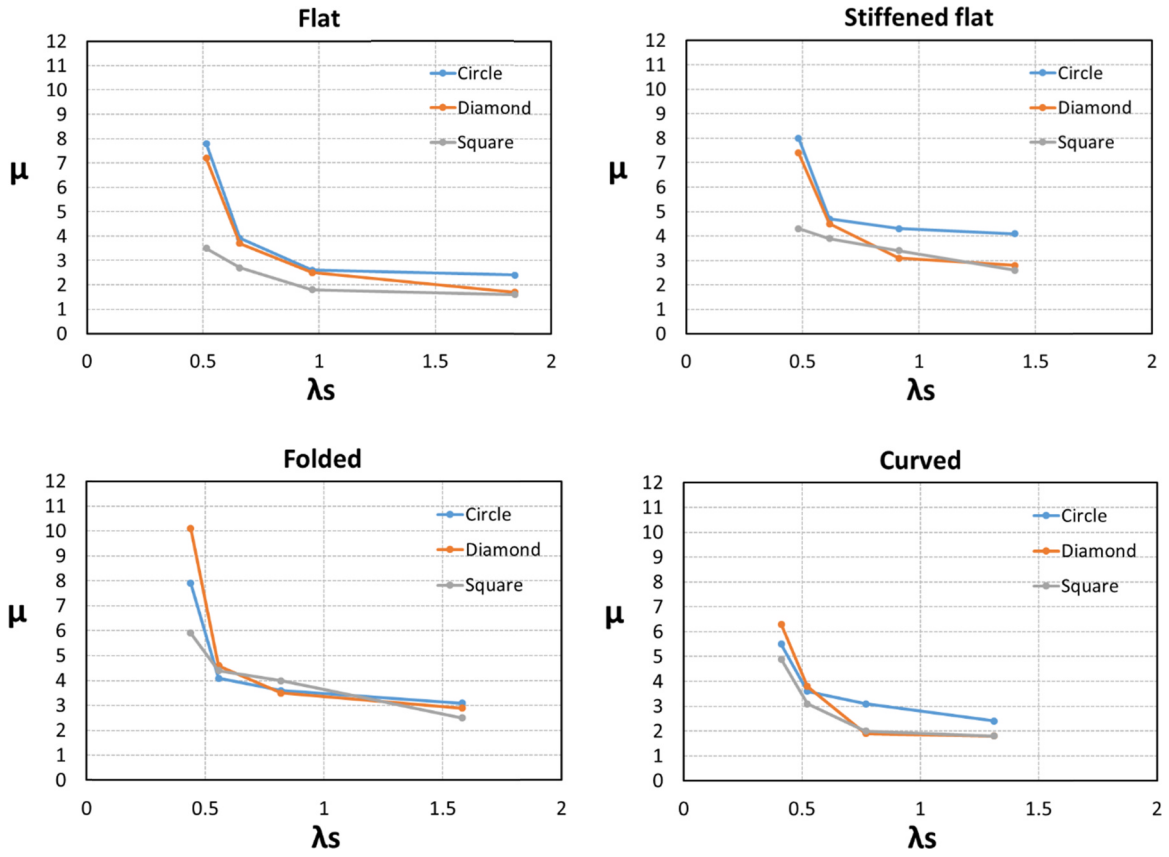

Fig. 20. Ductility of CFS connections as a function of slenderness ratio and bolt arrangement.

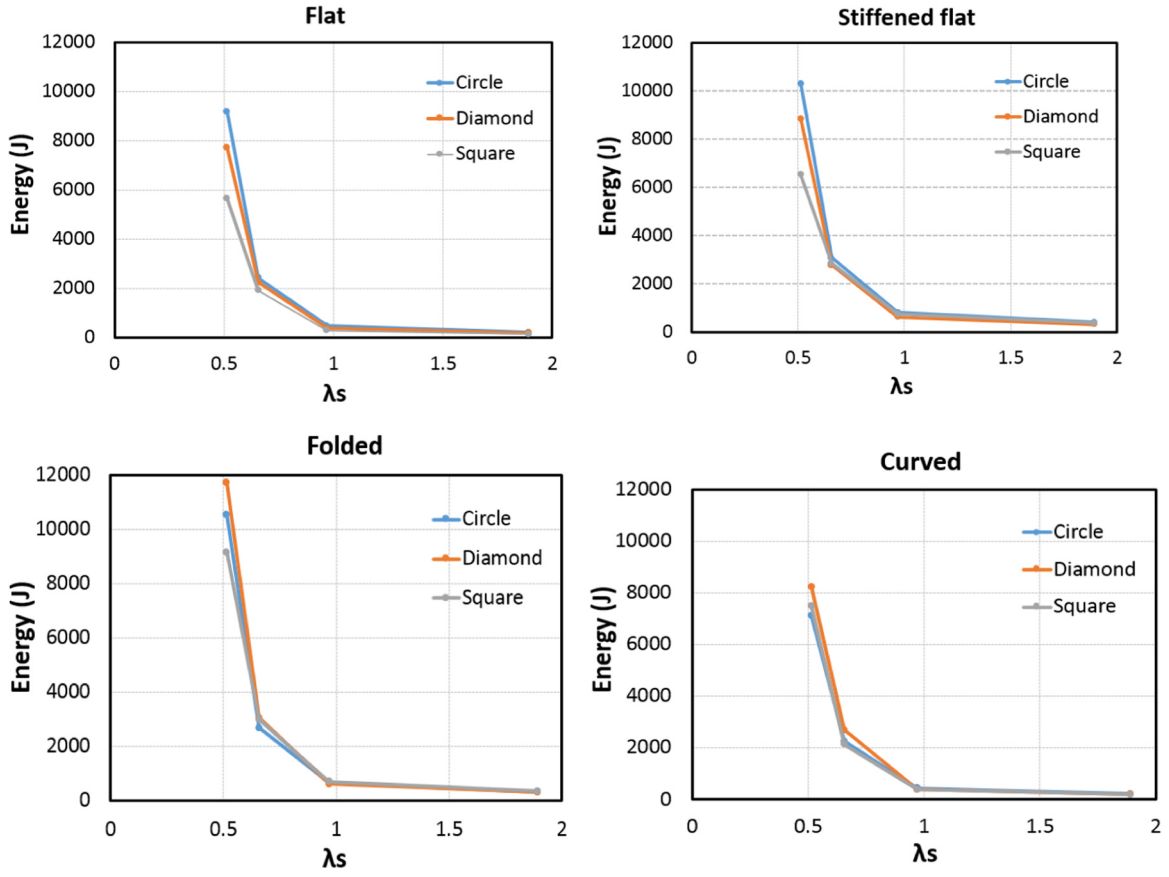

Fig. 21. Energy dissipation capacity of CFS connections as a function of slenderness ratio and bolt arrangement.

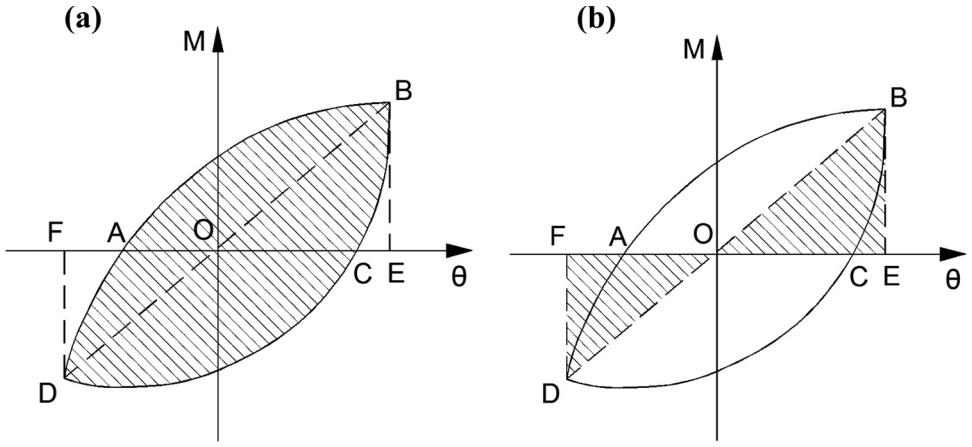

Fig. 22. Definition of the damping coefficient.

5.8. Damping coefficient

The equivalent viscous damping coefficient, h_e, is another indicator of the energy dissipation capability for seismic applications [56,57]. This parameter represents the plumpness of the hysteresis loop and can be calculated using the following equation:

$$h_e = \frac{1}{2\pi}\frac{S_{\Delta ABC} + S_{\Delta CDA}}{S_{\Delta OBE} + S_{\Delta ODF}} \tag{6}$$

where $S_{\Delta ABC} + S_{\Delta CDA}$ is the energy dissipated by the connection at the expected rotation (shaded area in Fig. 22(a)). $S_{\Delta OBE} + S_{\Delta ODF}$ is the total strain energy of the connection at the expected rotation, in which the connection is assumed to remain elastic (shaded area in Fig. 22(b)). Points B and D represent the maximum positive and negative moment capacities of a loop, respectively.

In this study, the equivalent viscous damping coefficients are calculated for two different loops based on the peak moment and the ultimate moment (20% drop from the peak moment in softening stage) of the connections as shown Fig. 23 and Fig. 24, respectively. The results in general indicate that connections with class 1 and 2 beam elements can provide higher equivalent viscous damping coefficients compared to other classes, and therefore, are suitable for seismic applications. It is shown that reducing the CFS beam cross-sectional slenderness is always accompanied by increasing the equivalent viscous damping coefficient, while the effect of cross-sectional shape on the damping coefficient is negligible. It can be also noted that the damping coefficients

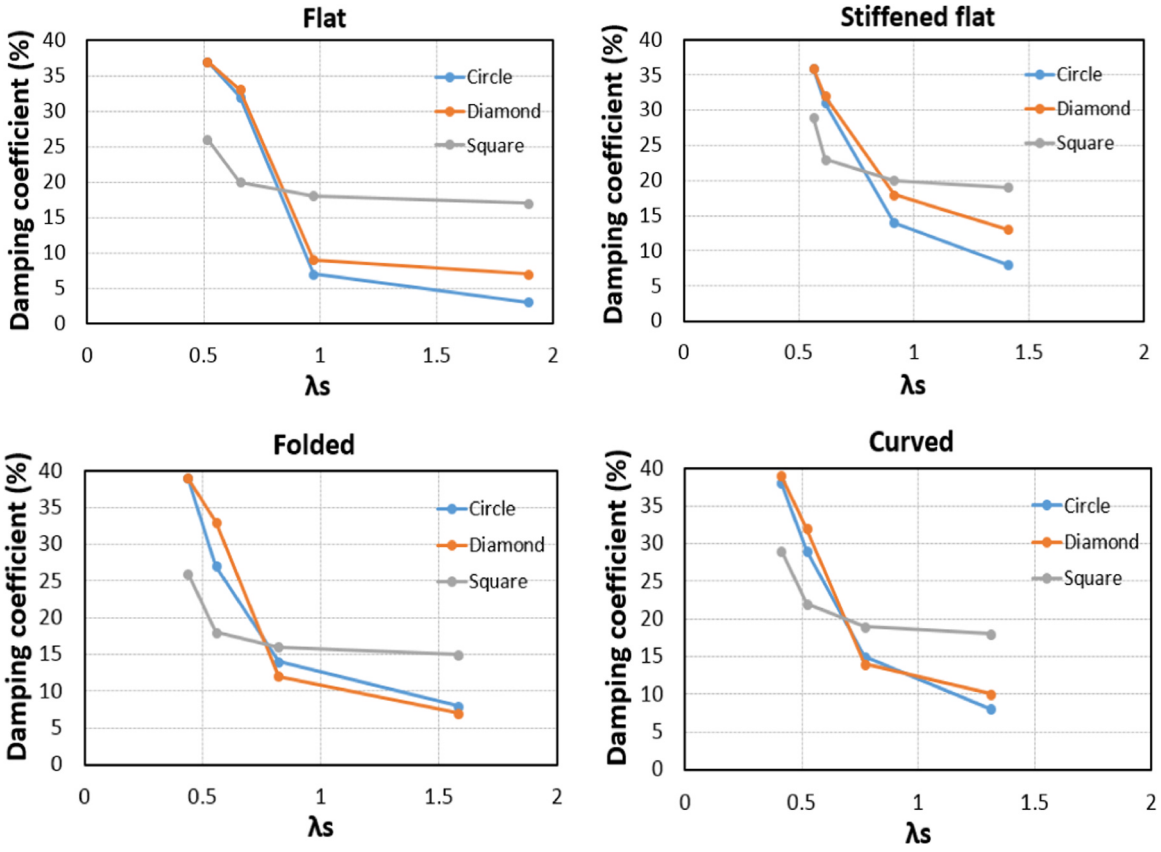

Fig. 23. Equivalent viscous damping coefficient at peak moment.

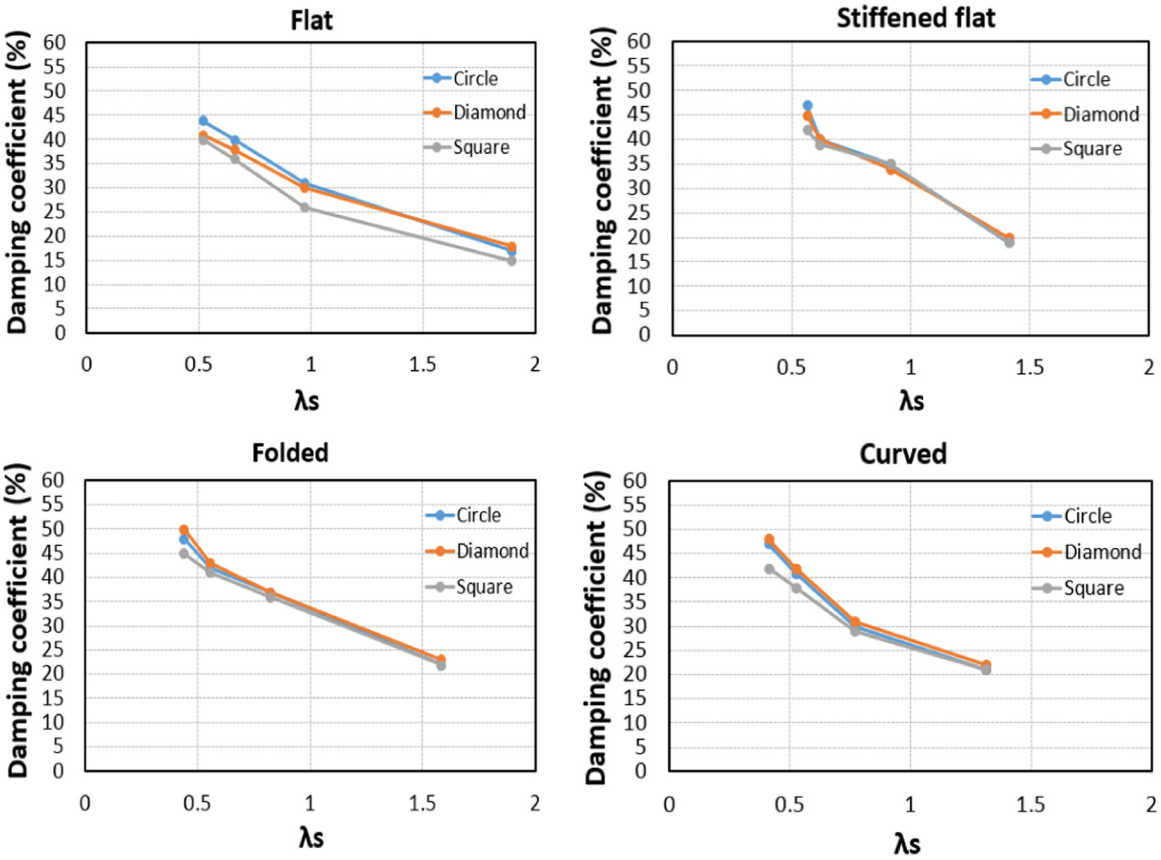

Fig. 24. Equivalent viscous damping coefficient at ultimate moment.

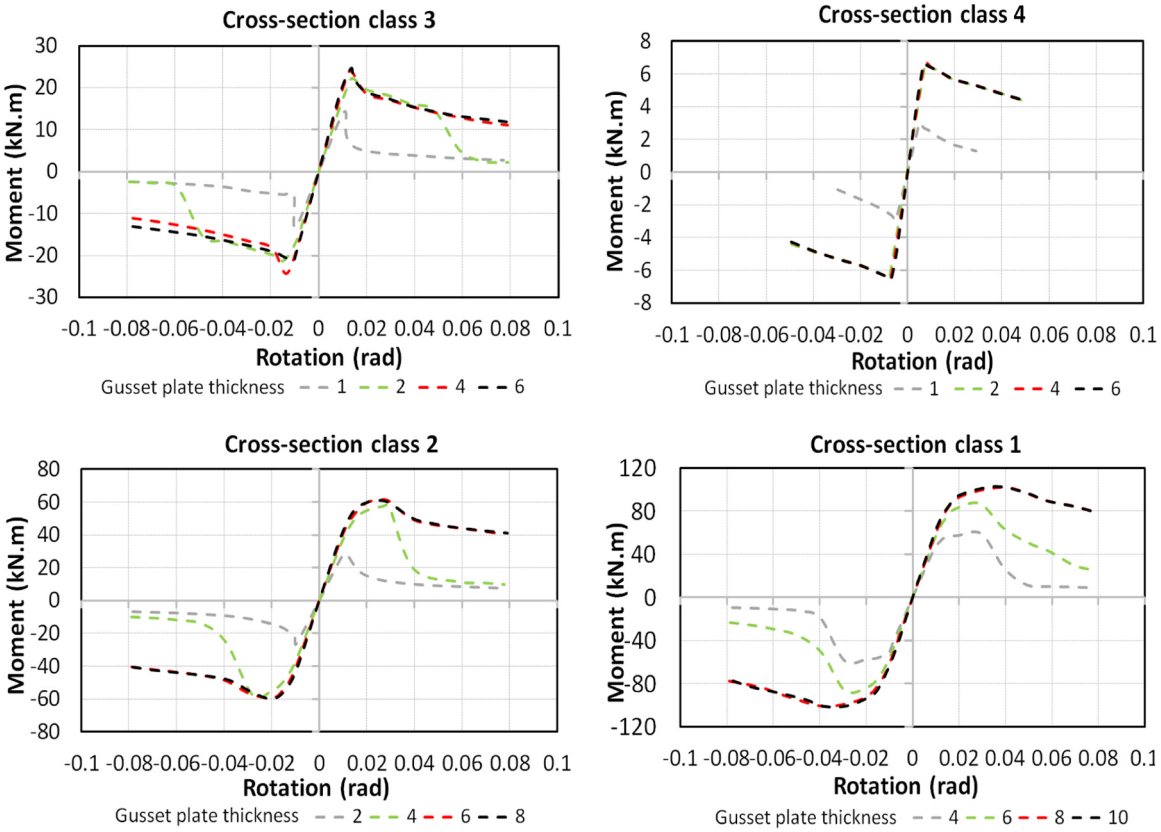

Fig. 25. Effect of gusset plate thickness on the moment-rotation behaviour of CFS connections.

corresponding to the peak moment (h_e) are always smaller (up to 15%) than those corresponding to the ultimate moment.

Fig. 23 shows that, up to the peak moment, diamond and circle bolt configurations are capable of dissipating more energy in the connections with class 1 and 2 beam sections. However, the square bolt arrangement provides better results for class 3 and 4 sections, which implies that the majority of the seismic energy is damped by the connection in the elastic stage (before buckling). The results in Fig. 24 indicate that the equivalent viscous damping coefficient at ultimate moment is not significantly affected by changing the bolt configuration.

5.9. Effect of gusset plate thickness

In general, previous studies indicated that the design of gusset plate in the stiffened end-plate bolted joints can influence the transfer mechanism of the forces and affect the cyclic rotational behaviour of the connections [38,39]. Therefore, in this section the effect of gusset plate thickness on the cyclic behaviour of the bolted-moment connection is investigated. Fig. 25 compares the moment-rotation curves of the connections with class 1–4 flat channel beam sections (see Table 1) using the square bolt configuration and various gusset plate thicknesses. In general, using gusset plates with the same or lower thickness as the CFS beam (1, 2, 4 and 6 mm thickness for class 4, 3, 2 and 1 sections, respectively) shifts the local buckling from the CFS beam to the gusset plate. As shown in Fig. 25, this premature failure mode can significantly reduce the moment capacity of the connections and lead to higher post-buckling strength degradations. This undesirable failure mode can be prevented by increasing the gusset plate thickness slightly above the thickness of the CFS beam.

6. Summary and conclusions

Experimentally validated FE models were developed by taking into account material nonlinearity and geometrical imperfections. A comprehensive parametric study was conducted on CFS bolted beam-to-column connections with gusset plates under cyclic loading to compare the efficiency of various design solutions for earthquake resistant frames. The following conclusions can be drawn:

(1) The dominant failure mode of the CFS bolted-moment connections is due to the local buckling of the CFS beam sections close to the first row of the bolts. Curved and folded flange channels can postpone the local buckling of the flange by creating an in-plane stiffness through arching action and shifting the local buckling failure to the web. However, using bent flange channels (folded and curved) can only increase the moment capacity of the connections by up to 10%.
(2) The slenderness of CFS beam elements and the arrangement of bolts govern the capacity of connections. In general, using a square bolt arrangement leads to a higher moment capacity (up to 32%) compared to the other arrangements examined.
(3) The bolted-moment connections with beam sections class 1 and 2 generally satisfy AISC requirements for Special Moment Resisting Frames (SMFs). Connections with beam class 2 are only acceptable when intermediate stiffeners are used in the flanges (stiffened flat), while connections with class 4 beam cross sections are not considered to be suitable for SMFs.
(4) The ductility of the connections is also governed by bolt arrangement and beam cross-sectional shape and slenderness ratio. Ductility is increased radically by decreasing the slenderness ratio of the CFS beam sections. For the same beam slenderness ratio and bolt arrangement, folded flange sections result in up to 55%, 45% and 30% higher ductility levels compared to the curved, flat and stiffened flat sections, respectively. While the best bolt arrangement is related to the beam slenderness ratio and cross-sectional shape, in general, using the circle and diamond bolt arrangements can increase the ductility of the connections (up to 100%) compared to the conventional square bolt arrangement.
(5) The effect of cross-sectional shape and bolt configuration on the energy dissipation capacity of the connections is only evident when class 1 beam sections are utilized. For these connections, using folded flange beam cross sections results in up to 250%, 200% and 150% higher energy dissipation capacity compared to flat, curved and stiffened flat sections, respectively. Using diamond and circle bolt arrangements could also considerably increase (up to 250%) the energy dissipation capacity of the connections compared to the conventional square bolt arrangement. It was shown that reducing the CFS beam cross-sectional slenderness is always accompanied by increasing the equivalent viscous damping coefficient, while the effect of cross-sectional shape on the equivalent damping coefficient is negligible.
(6) Using gusset plates with the same or lower thickness as the CFS beam may lead to a premature failure mode in the gusset plate and considerably reduce the moment capacity of the connection. However, this failure mode can be efficiently prevented by increasing the gusset plate thickness slightly above the thickness of the CFS beam.

Acknowledgement

This work was supported by the Engineering and Physical Sciences Research Council (EPSRC) in the UK, through grant number EP/L019116/1. The authors would like to thank the EPSRC for their financial support.

References

[1] L. Fiorino, O. Iuorio, R. Landolfo, Designing CFS structures: the new school bfs in naples, Thin Wall Struct. 78 (2014) 37–47.
[2] H. Moghimi, H.R. Ronagh, Performance of light-gauge cold-formed steel strap-braced stud walls subjected to cyclic loading, Eng. Struct. 31 (2009) 69–83.
[3] S.-H. Lin, C.-L. Pan, W.-T. Hsu, Monotonic and cyclic loading tests for cold-formed steel wall frames sheathed with calcium silicate board, Thin-Walled Struct. 74 (2014) 49–58.
[4] M. Zeynalian, H.R. Ronagh, S. Hatami, Seismic characteristics of K-braced cold-formed steel shear walls, J. Constr. Steel Res. 77 (2012) 23–31.
[5] Z. Xu, Z. Chen, B.H. Osman, S. Yang, Seismic performance of high-strength light-weight foamed concrete-filled cold-formed steel shear walls, J. Constr. Steel Res. 143 (2018) 148–161.
[6] L. Fiorino, M.T. Terracciano, R. Landolfo, Experimental investigation of seismic behaviour of low dissipative CFS strap-braced stud walls, J. Constr. Steel Res. 127 (2016) 92–107.
[7] L. Fiorino, O. Iuorio, R. Landolfo, Designing CFS structures: the new school bfs in naples, Thin Wall Struct. 78 (2014) 37–47.
[8] J.B.P. Lim, D.A. Nethercot, Finite element idealization of a cold-formed steel portal frame, J. Struct. Eng. 130 (2004) 78–94.
[9] J.B.P. Lim, D.A. Nethercot, Ultimate strength of bolted moment-connections between cold-formed steel members, Thin Wall Struct. 41 (2003) 1019–1039.
[10] J.B. Lim, G.J. Hancock, G.C. Clifton, C.H. Pham, R. Das, DSM for ultimate strength of bolted moment-connections between cold-formed steel channel members, J. Constr. Steel Res. 117 (2016) 196–203.
[11] S.M. Mojtabaei, M.Z. Kabir, I. Hajirasouliha, M. Kargar, Analytical and experimental study on the seismic performance of cold-formed steel frames, J. Constr. Steel Res. 143 (2018) 18–31.
[12] A. Bagheri Sabbagh, M. Petkovski, K. Pilakoutas, R. Mirghaderi, Experimental work on cold-formed steel elements for earthquake resilient moment frame buildings, Eng. Struct. 42 (2012) 371–386.
[13] B.P. Gilbert, K.J.R. Rasmussen, Bolted moment connections in drive-in and drive-through steel storage racks, J. Constr. Steel Res. 66 (2010) 755–766.
[14] C.M. Uang, A. Sato, J.K. Hong, K. Wood, Cyclic testing and modeling of cold-formed steel special bolted moment frame connections, J. Struct. Eng. 136 (2010) 953–960.
[15] M.H. Serror, E.M. Hassan, S.A. Mourad, Experimental study on the rotation capacity of cold-formed steel beams, J. Constr. Steel Res. 121 (2016) 216–228.
[16] Ž. Bučmys, A. Daniūnas, Analytical and experimental investigation of cold-formed steel beam-to-column bolted gusset-plate joints, J. Civil. Eng. Manag. 21 (2015) 1061–1069.
[17] J.B.P. Lim, D.A. Nethercot, Ultimate strength of bolted moment-connections between cold-formed steel members, Thin Wall Struct. 41 (2003) 1019–1039.
[18] M.F. Wong, K.F. Chung, Structural behaviour of bolted moment connections in cold-formed steel beam-column sub-frames, J. Constr. Steel Res. 58 (2002) 253–274.
[19] B. Calderoni, A. De Martino, A. Formisano, L. Fiorino, Cold formed steel beams under monotonic and cyclic loading: Experimental investigation, J. Constr. Steel

Res. 65 (2009) (1548-1548).
[20] D.A. Padilla-Llano, C.D. Moen, M.R. Eatherton, Cyclic axial response and energy dissipation of cold-formed steel framing members, Thin-Walled Struct. 78 (2014) 95–107.
[21] D.A. Padilla-Llano, M.R. Eatherton, C.D. Moen, Cyclic flexural response and energy dissipation of cold-formed steel framing members, Thin-Walled Struct. 98 (2016) 518–532.
[22] A. Bagheri Sabbagh, M. Petkovski, K. Pilakoutas, R. Mirghaderi, Development of cold-formed steel elements for earthquake resistant moment frame buildings, Thin-Walled Struct. 53 (2012) 99–108.
[23] J. Ye, I. Hajirasouliha, J. Becque, K. Pilakoutas, Development of more efficient cold-formed steel channel sections in bending, Thin-Walled Struct. 101 (2016) 1–13.
[24] J. Ye, J. Becque, I. Hajirasouliha, S.M. Mojtabaei, J.B.P. Lim, Development of optimum cold-formed steel sections for maximum energy dissipation in uniaxial bending, Eng. Struct. 161 (2018) 55–67.
[25] M.H. Serror, E.M. Hassan, S.A. Mourad, Experimental study on the rotation capacity of cold-formed steel beams, J. Constr. Steel Res. 121 (2016) 216–228.
[26] J.B.P. Lim, D.A. Nethercot, Stiffness prediction for bolted moment-connections between cold-formed steel members, J. Constr. Steel Res. 60 (2004) 85–107.
[27] A. Bagheri Sabbagh, M. Petkovski, K. Pilakoutas, R. Mirghaderi, Cyclic behaviour of bolted cold-formed steel moment connections: fe modelling including slip, J. Constr. Steel Res. 80 (2013) 100–108.
[28] I. Elkersh, Experimental investigation of bolted cold formed steel frame apex connections under pure moment, Ain Shams Eng. J. 1 (2010) 11–20.
[29] Ž. Bučmys, G. Šaučiuvėnas, The behavior of cold formed steel structure connections, Eng. Struct. Technol. 5 (2013) 113–122.
[30] F. Öztürk, S. Pul, Experimental and numerical study on a full scale apex connection of cold-formed steel portal frames, Thin-Walled Struct. 94 (2015) 79–88.
[31] J.B.P. Lim, D.A. Nethercot, Finite element idealization of a cold-formed steel portal frame, J. Struct. Eng. 130 (2004) 78–94.
[32] Abaqus/CAE User's Manual, version 6.7, USA, 2007.
[33] R. Gutierrez, A. Loureiro, J.M. Reinosa, M. Lopez, Numerical study of purlin joints with sleeve connections, Thin-Walled Struct. 94 (2015) 214–224.
[34] Q. Liu, J. Yang, F.L. Wang, Numerical simulation of sleeve connections for cold formed steel sigma sections, Eng. Struct. 100 (2015) 686–695.
[35] Eurocode 3:, design of steel structures: Part 1.1: General rules and rules for buildings, EN 1993-1-1, 2005.
[36] M. D'Aniello, D. Cassiano, R. Landolfo, Monotonic and cyclic inelastic tensile response of European preloadablegr10.9 bolt assemblies, J. Constr. Steel Res. 124 (2016) 77–90.
[37] M. D'Aniello, D. Cassiano, R. Landolfo, Simplified criteria for finite element modelling of European preloadable bolts, Steel Compos. Struct., Int. J. 24 (2017) 643–658.
[38] M. D'Aniello, R. Tartaglia, S. Costanzo, R. Landolfo, Seismic design of extended stiffened end-plate joints in the framework of Eurocodes, J. Constr. Steel Res. 128 (2017) 512–527.
[39] R. Tartaglia, M. D'Aniello, G.A. Rassati, J.A. Swanson, R. Landolfo, Full strength extended stiffened end-plate joints: aisc vs recent European design criteria, Eng. Struct. 159 (2018) 155–171.
[40] M.R. Haidarali, D.A. Nethercot, Finite element modelling of cold-formed steel beams under local buckling or combined local/distortional buckling, Thin-Walled Struct. 49 (2011) 1554–1562.
[41] H. Wang, Y. Yan, M. Wan, X. Wu, Experimental investigation and constitutive modeling for the hardening behavior of 5754O aluminum alloy sheet under two-stage loading, Int. J. Solids Struct. 49 (2012) 3693–3710.
[42] R.K. Boger, Non-Monotonic Strain Hardening and Its Constitutive Representation (Ph.D. thesis), The Ohio State University, 2006.
[43] L.-J. Jia, T. Koyama, H. Kuwamura, Prediction of cyclic large plasticity for pre-strained structural steel using only tensile coupon tests, Front. Struct. Civil. Eng. 7 (2013) 466–476.
[44] J. Ye, S.M. Mojtabaei, I. Hajirasouliha, Local-flexural interactive buckling of standard and optimised cold-formed steel columns, J. Constr. Steel Res. 144 (2018) 106–118.
[45] J. Ye, S.M. Mojtabaei, I. Hajirasouliha, P. Shepherd, K. Pilakoutas, Strength and Deflection Behaviour of Cold-Formed Steel Back-to-Back Channels, Eng. Struct. (2018) (In press).
[46] B.W. Schafer, T. Peköz, Computational modeling of cold-formed steel: characterizing geometric imperfections and residual stresses, J. Constr. Steel Res. 47 (1998) 193–210.
[47] A.C. Walker, Design and Analysis of Cold-formed Sections, Halsted Press, 1975.
[48] ANSI/AISC, 341-16, Seismic provisions for structural steel buildings, american institute of steel construction (AISC), 2016.
[49] A. Bagheri Sabbagh, Cold-formed steel elements for earthquake resistant moment frame buildings (Ph.D. thesis), University of Sheffield, 2011.
[50] CEN, Eurocode 3: Design of Steel Structures. Part 1-1: General Rules and Rules for Buildings, European Comittee for Standardization, Brussels, 2005.
[51] C. Eurocode, 3: design of steel structures part 1–12: additional rules for the extension of EN 1993 up to steel grades *S* 700, London (UK): British Standards Institution, BS EN 1-12, 1993.
[52] S. Ádány, B. Schafer, Buckling mode decomposition of single-branched open cross-section members via finite strip method: derivation, Thin-Walled Struct. 44 (2006) 563–584.
[53] S. Ádány, B.W. Schafer, Generalized constrained finite strip method for thin-walled members with arbitrary cross-section: secondary modes, orthogonality, examples, Thin-Walled Struct. 84 (2014) 123–133.
[54] Z. Li, B.W. Schafer, Buckling analysis of cold-formed steel members with general boundary conditions using CUFSM conventional and constrained finite strip methods, 2010.
[55] FEMA-356, Pre Standard and Commentary for the Seismic Rehabilitation of Buildings, American Society Of Civil Engineers, USA, Virginia, 2000.
[56] K.K. Wijesundara, R. Nascimbene, T.J. Sullivan, Equivalent viscous damping for steel concentrically braced frame structures, Bull. Earthq. Eng. 9 (5) (2011) 1535–15558.
[57] M.A. Bezabeh, S. Tesfamariam, S.F. Stiemer, Equivalent viscous damping for steel moment-resisting frames with cross-laminated timber infill walls, J. Struct. Eng. 142 (1) (2016) 1–12.